An-Najah University Journal for Research – A

Natural Sciences

Tidal Wave Amplification and Phase Shift from the Entrance of Khor Abdullah to the Shatt Al-Basrah Regulator, Northern Arabian Gulf

Ali A. Lafta [1,*], Faez Y. Aleedani[1] & Abather J. Alhallaf[1,2]

Type: Full Article. Received: 22nd Feb. 2025, Accepted: 16th Aug. 2025, Published: ×××× DOI: ××××

Accepted Manuscript, In Press

Abstract: This study investigates tidal-wave amplification and phase shift along a propagation path from the northern Arabian Gulf to the Shatt Al-Basrah Regulator (Basrah Province, southern Iraq). We analyze a continuous one-year (2022) record of hourly water-level measurements from two stations located at the entrance of Khor Abdullah and at the Shatt Al-Basrah Regulator. Harmonic analysis was performed using the MATLAB WorldTide toolbox for tidal and tidal-current analysis and prediction. Results show a northward increase in maximum water level, accompanied by progressive amplification of tidal-wave amplitude and an increase in tidal range. At the regulator, the maximum water level is approximately 0.5 m higher than at the Khor Abdullah entrance. Among the resolved constituents, the principal lunar semidiurnal constituent (M2) has the largest amplitude at both stations and increases by ~100% between them. A phase lag of 52.19° (≈108 min) indicates that high tide at the Shatt Al-Basrah Regulator occurs nearly two hours later than at the entrance to Khor Abdullah. These findings provide insight into tidal-wave transformation in the northern Arabian Gulf and may help improve navigation safety, coastal infrastructure planning, and studies of sediment dynamics in the region.

Keywords: Coastal hydrodynamics, Environment, tidal wave, Arabian Gulf.

Introduction

Understanding tidal-wave propagation in coastal and estuarine environments is critical for navigation, port operations, and coastal infrastructure planning, and it also supports assessments of sediment transport and flood risk in low-lying regions. Shallow coastal systems are strongly influenced by tidal forcing, which drives water-level variability and controls inundation and drainage across intertidal areas. Variations over the tidal cycle can flood adjacent wetlands, supporting sediment transport, nutrient exchange, and habitat availability [1-3]. In these environments, changes in local water level are reflected in measurable variations in the amplitudes and phases of tidal constituents; in turn, these variations can influence water temperature, near-surface air temperature, and relative humidity, highlighting coupled tidal–meteorological interactions [4-5].

Tidal forces drive water-level variability and current dynamics that shape shoreline morphology and ecological conditions, particularly in environments influenced by shallow-water processes and tidal constituents [6,7]. In shallow, constricted waterways, tidal characteristics can be significantly modified by bottom friction, channel geometry, and bathymetric changes, leading to variations in tidal amplitude, range, and timing [8]. Tidal waves, generated primarily by the gravitational forcing of the Moon and the Sun, undergo substantial transformation as they propagate toward coastal and estuarine environments due to shallow-water effects [9]. These effects alter key characteristics such as amplitude, propagation speed, and tidal range, depending largely on the depth, geometry, and seabed topography of the waterway [8]. In shallow channels, tidal waves may be fully reflected, partially reflected, or continue propagating with reduced energy as a result of bottom friction [10,11]. Tidal energy is transmitted across multiple frequencies, reflecting the complex orbital interactions between the Moon, Earth, and Sun. If both the lunar and solar orbits were perfectly circular and aligned with the Earth's equator, tidal energy would be confined to two primary semi-diurnal constituents—lunar (M2) and solar (S2) [12]. However, because both orbits are elliptical, their distances vary over time, and their orbital planes are inclined relative to the equator, tidal energy is spread across a broader spectrum of constituents [13]. These constituents are commonly classified by their celestial origin (lunar or solar) and temporal characteristics, including diurnal, semidiurnal, and long-period constituents, as well as shallow-water constituents such as overtides and compound tides that arise from nonlinear hydrodynamic interactions in bays and estuaries [14-17].

Oceanographic research in the northwestern Arabian Gulf, particularly within Khor Abdullah, Khor Al-Zubair, and the Shatt Al-Basrah Canal, remains scarce—especially studies using continuous, long-term measurements. Several observational and modeling studies have examined tidal dynamics in the northwestern Arabian Gulf and adjacent estuaries. Field-based harmonic analyses and one-year water level records have characterized tidal constituents and tidal asymmetry within Khor Abdullah, Khor Al-Zubair, and the Shatt Al-Arab estuary, identifying M2 as the dominant constituent and documenting spatial changes in tidal amplitude and range [17,18]. Numerical hydrodynamic models (e.g., MIKE11, Mike 21) have also been applied to simulate tidal propagation and to assess prospective impacts such as sea-level rise on water levels [18] . Despite

1 Marine Science Center, University of Basrah, Iraq
* Corresponding author email: ali.lafta@uobasrah.edu.iq
2 Boone Pickens School of Geology, Oklahoma State University, USA

these contributions, long-term observational datasets that simultaneously quantify tidal-wave amplification and phase lag between the entrance of Khor Abdullah and the Shatt Al-Basrah Regulator remain scarce. Accordingly, this study addresses this gap by analyzing tidal-wave amplification and phase shift along the propagation pathway from the entrance of Khor Abdullah to the Shatt Al-Basrah Regulator using a continuous one-year record of hourly water-level observations collected at strategically located stations.

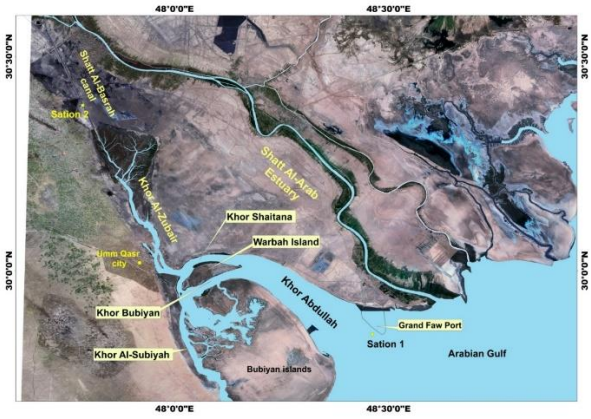

Figure (1): Map of the study area and the locations of measurement stations.

Materials and Methods

Study Area

Khor Abdullah is funnel-shaped and extends approximately 40 km in a northwestward direction until it reaches the southern part of Warbah Island, where it branches into Khor Bubiyan, connecting it to Khor Al-Subiyah and Khor Shaitana [18]. Khor Shaitana serves as a link between Khor Abdullah and Khor Al-Zubair, as illustrated in Figure (1). The eastern bank of Khor Abdullah has a moderate slope, whereas the western bank, represented by the shores of Warbah and Bubiyan islands, has a steeper slope. As a result, the international navigation channel in Khor Abdullah is located closer to the Kuwait side. Water depths in Khor Abdullah range from 7 to 14 m, with an average depth of approximately 10 m [18,19]. The channel has an average width of 17 km at its southern entrance, where it meets the Arabian Gulf, but narrows northward to 6.5 km south of Warbah Island Figure (1). The salinity of Khor Abdullah reaches 38 psu, classifying it as a high-salinity bay [20]. It is characterized by strong tidal currents during both the spring and ebb phases [21,22].

On the other hand, Khor Al-Zubair is located in southwestern Iraq and connects to the Arabian Gulf through Khor Shaitana and Khor Abdullah, making it a natural extension of the Arabian Gulf [18]. The total length of Khor Al-Zubair is approximately 40 km, with its lower boundary located about 8 km south of Umm Qasr city and north of Warbah Island. The upper boundary of Khor Al-Zubair branches into multiple smaller channels, forming a tree-like pattern, as shown in Figure (1). Khor Al-Zubair has an average width of approximately 1 km, with navigational channel depths ranging from 10 to 20 m. The total surface area covered by water during a spring tide is approximately 60 km² [18]. Shatt Al-Basrah Canal was constructed in 1983 as an artificial drainage canal to discharge flood waters from the Euphrates River into the Arabian Gulf via Khor Al-Zubair. This canal is approximately 37 km long, extending from its connection with the Karmah Ali River to the upper reaches of Khor Al-Zubair. Due to reduced discharge from the Euphrates River, a new hydraulic connection for the canal was constructed [23]. In 1993, its connection was modified to divert water into the Main Outfall Drain (MOD), which is designed for draining agricultural wastewater from the Euphrates basin. Seawater intrusion is controlled by the Shatt Al-Basrah Regulator, which is located approximately 22 km upstream toward Khor Al-Zubair Figure (1). However, in recent years, agricultural wastewater has been redirected toward the marshes, significantly reducing the flow reaching Shatt Al-Basrah. Currently, the discharge rate is very low, not exceeding 10 m3/sec.

Used Data

The present study relies on field measurements of water-level fluctuations collected at two locations. The first location is at the entrance of Khor Abdullah, near the western breakwater of the Grand Faw Port. The second location is located upstream near the Shatt Al-Basrah Regulator, as shown in Figure (1). Water-level data at Station 1 were obtained using a HOBO tide gauge installed at the Shatt Al-Basrah Regulator. Data at Station 2 were provided by the General Company for Ports of Iraq (GCPI) in collaboration with Daewoo Engineering & Construction, which constructed the western breakwater of the Grand Faw Port [24]. An automated monitoring station was established to record various oceanographic variables and is located approximately 650 m from the western breakwater of the Grand Faw Port Figure (1). Both datasets were referenced to Iraq's official vertical datum (Faw 1979 Datum), which represents the mean sea level in Al-Faw city [18]. Water-level records at Station 1 were interrupted for several days due to a temporary malfunction of the tide gauge.

Harmonic Analysis

The analysis of recorded sea-level data in the study area was conducted using the MATLAB WorldTide program. This software applies harmonic analysis using the least-squares method to determine the tidal constants of the constituents used in sea level data analysis. The program includes between 5 and 35 tidal constituent**s** in the harmonic model [9]. Harmonic analysis represents periodic functions as a linear superposition of fundamental waves and extends the concept of Fourier series. Sea-level fluctuations resulting from various forcing mechanisms can be expressed as the sum of a series of simple harmonic terms, also known as tidal constituents. Each term can be represented as a sinusoidal wave with a known frequency linked to the periodic motion of the Earth-Moon-Sun system. The primary objective of harmonic analysis is to determine tidal constants, including the amplitude and phase of each sinusoidal component affecting sea-level variability in a given region. These constants can then be used to predict future tidal behavior for that location. The fundamental equation for the harmonic model is written as follows [9]:

$$h(t) = h_{\circ} + \sum_{j=1}^{m} f_j H_j \cos(w_j t + u_j - k_j^*) \quad (1)$$

where h(x,t) represents the water level computed using the harmonic model; t is time; is the mean water level in the study area; fj is the lunar node factor for the amplitude of the jth tidal constituent; Hj is the amplitude of the jth tidal constituent; ωj is the frequency of the jth tidal constituent; uj is the nodal phase; k*j is the phase lag; and m is the number of tidal constituents used in the model. For purely solar tidal constituents, fj is taken as 1 and uj is set to 0.

Results and Discussion

As the tidal wave propagates from the northwestern of the Arabian Gulf toward the Shatt Al-Basrah canal system, it undergoes amplification and distortion due to local hydrodynamic processes. The water level fluctuations shown in Figure (2) indicate a noticeable increase in the Higher High Water (HHW) as the tidal wave propagates northward. At the

upper reaches of the study area (Shatt Al-Basrah regulator), the HHW reaches approximately 2.25 m, which is more than 0.5 m higher than at the lower reaches (Khor Abdullah entrance). The highest recorded HHW values during the study period were 1.98 m at Station 1 and 2.25 m at Station 2. Meanwhile, the recorded Lower Low Water (LLW) values were −2.78 m at Station 1 and −3.45 m at Station 2. This variation in extreme water levels is attributed to local hydrodynamics and the convergent geometry of the study area. As the cross-sectional area gradually decreases from the Arabian Gulf toward the upper reaches of the Shatt Al-Basrah Canal, incoming tidal energy becomes concentrated within a narrower region. This concentration leads to amplification of tidal-wave amplitude and an increase in tidal range.

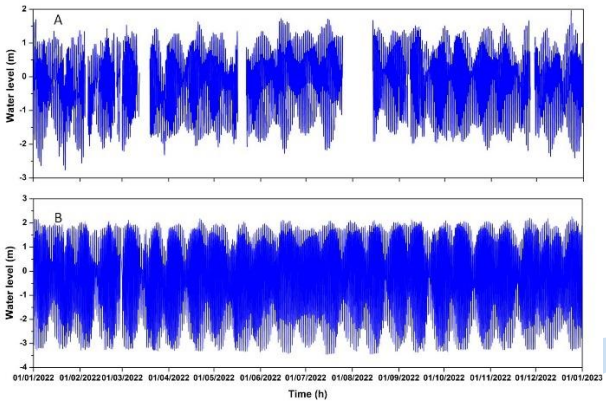

Figure (2): Time series of water level fluctuations during the year 2022 at (A) Khor Abdullah entrance and (B) Shatt Al-Basrah regulator.

Figure (2) shows that there are no significant seasonal fluctuations in water level heights. However, due to the elliptical orbit of the Moon and modulation of the M2 tidal constituent by variations in lunar gravitational forcing, noticeable differences occur between successive spring and neap tidal cycles. Figure (3) compares observed and estimated water levels generated by the harmonic model at stations 1 and 2. The harmonic model performs well at both stations, with agreement levels of 93.2% and 94.63% and root mean square errors of 0.22 m and 0.36 m at Stations 1 and 2, respectively. Using the harmonic model (MATLAB WorldTide), 35 tidal constituents were identified and classified as diurnal, semi-diurnal, and shallow water constituents. Shallow-water constituents, such as overtides and compound tidal constituents, are generated through nonlinear interactions between the primary tidal waves and the seabed [25,26]. The amplitude of semi-diurnal constituents M2, S2, and N2 is amplified from the Khor Abdullah inlet to upstream, as shown in Table 1, in response to the influence of local hydrodynamics. The amplification of the tidal constituents' amplitudes is caused by a balance between geometric amplification, which occurs when the cross-sectional area decreases in the upstream direction, and frictional dissipation. The results showed that the highest amplitude value was for the M2 constituent at two study stations. Its amplitude increases in the upper reaches of the study area by approximately 100% compared to its value at the Khor Abdullah entrance. It was also found that there is a significant increase in the amplitudes of the principal semidiurnal tidal constituents (S2 and N2), accompanied by a slight increase in the amplitude of the principal diurnal constituent (K1) and a slight decrease in the amplitude of the diurnal tidal constituent (O1) as we move northward toward the upper reaches of the study area. Percentage increases in amplitude were 102% for S2, 100% for N2, and 13% for K1. Meanwhile, the O1 constituent decreased by 7% at Station 2 compared to its value at Station 1. Amplification of tidal constituents in the study region is attributed to the convergent geometry of the channel, which overcomes frictional dissipation along the bed. The primary contributor in all stations was the principal lunar semidiurnal constituent (M2), accounting for 30% at Station 1 and 31% at Station 2. The contributions of other principal tidal constituents were as follows, principal solar semidiurnal constituent (S2) is 10.1% and 10.5%, lunar semidiurnal constituent (N2) is 5.9% and 6.1%, diurnal constituent (K1) is 16.5% and 9.5%, diurnal constituent (O1) is 9.8% and 4.6% at station 1 and station 2, respectively. The fluctuation in maximum tidal wave amplitude and the contribution of each tidal constituent differs from one location to another, depending on various natural factors, primarily bathymetric characteristics and the shape of the waterway. This is particularly evident at Station 1, which has a larger cross-sectional area compared to the station 2. Similarly, our results show that the diurnal constituent P1, which has a major contribution to water level variation in the Arabian Gulf, as reported by Pous et al. (2012) [27], has an amplitude reduction of roughly 16% in the upstream of the study area. Constructive or destructive interference, created due to the non-interaction of P1 with K1 and O1 further amplifies or dampens the P1 component. A combination of factors, including reduced water outflow, bathymetric gradients, and frictional effects, likely contributes to the observed reduction in P1 amplitude toward the upstream reaches of the study area. Similar frictional damping of the P1 constituent has been reported in the Han River estuary, attributed to sediment loads and local bathymetric conditions [28].

Shallow water tidal constituents are raised by nonlinear interactions between primary astronomical tides and typically occur at higher harmonic frequencies. These constituents play a key role in shallow-water effects within tidal streams and estuarine environments. The results show amplification of several shallow-water constituents, including M3, MN4, M4, MS4, S4, 2MN6, M6, 2M6, S6, M8, and 3M8 from the inlet toward the upstream reaches of the study region. The amplification is attributed to nonlinear interactions among primary tidal constituents that generate overtides at higher harmonic frequencies [29]. Such amplification may result from combined of hydrodynamic factors on tidal propagation within Khor Abdullah, Khor Al-Zubair, and the Shatt Al-Basrah canal. In particular, strong tidal currents and irregular bathymetry can promote the formation of compound tides and overtides, enhancing higher harmonic components upstream [10]. Similar amplification of shallow-water constituents has been documented in other systems; for example, converging geometry and shallow depths have been shown to increase the amplitude of M4 in the Gulf of Khambhat, Arabian Sea [30], while bathymetric and geometric controls have led to tidal amplification in the Elbe estuary [31].

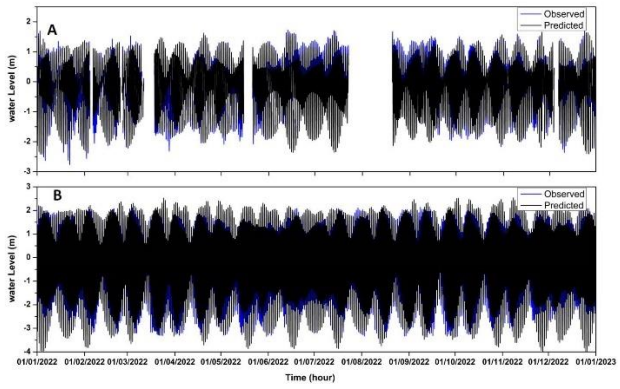

Figure (3): comparison between observed and estimated water level at A: station 1 and B: station 2.

Table (1): Amplitude and phase for the tidal constituent in the studied area.

Seq.	Tidal Constituent	Station 1		Station 2	
		Amplitude (m)	Phase (deg)	Amplitude (m)	Phase (deg)
1	Q1	0.058	154.91	0.051	167.5
2	RHO1	0.014	209.27	0.007	242.33
3	O1	0.304	231.46	0.282	240.03
4	M1	0.011	209.19	0.025	169.32
5	P1	0.142	308.05	0.122	347.87
6	S1	0.033	257.8	0.053	288.57
7	K1	0.51	293.35	0.576	323.69
8	J1	0.017	37.32	0.04	141.38
9	OO1	0.017	203.1	0.026	298.64
10	MNS2	0.011	311.29	0.077	214.77
11	2N2	0.031	49.97	0.065	65.84
12	MU2	0.027	6.51	0.265	323.11
13	N2	0.182	188.84	0.369	223.39
14	NU2	0.058	281.44	0.092	292.37
15	M2	0.93	271.15	1.864	323.34
16	LAM2	0.021	117.19	0.123	103
17	L2	0.044	302.41	0.149	321.17
18	T2	0.026	28.59	0.026	83.7
19	S2	0.314	26.05	0.637	101.58
20	R2	0.01	235.39	0.041	43.81
21	K2	0.118	181.64	0.179	250.35
22	2SM2	0.015	308.62	0.097	346.45
23	2MK3	0.037	86.17	0.142	105.67
24	M3	0.012	66.99	0.023	84.91
25	MK3	0.045	151.73	0.017	159.61
26	MN4	0.013	37.83	0.096	13.44
27	M4	0.036	127.66	0.218	117.78
28	MS4	0.026	227.17	0.169	250.51
29	S4	0.002	336.85	0.038	75.98
30	2MN6	0.003	77.23	0.025	257.6
31	M6	0.004	166.08	0.04	1.43
32	2M6	0.004	236.11	0.055	123.37
33	S6	0.001	123.23	0.007	109.51
34	M8	0.001	38.42	0.008	186.08
35	3M8	0.002	111.34	0.012	269.91

The percentage contribution of various constituent types in the estimated water level variation is as follows, semidiurnal constituents was 58.04% at the station 1 and 66.2% at the station 2, while diurnal frequencies contributed 35.9% and 19.3% at the station 1 and station 2, respectively. Additionally, there is a noticeable increase in the contribution of shallow water constituents, i.e., quarter-diurnal and sixth-diurnal as the tidal wave moves toward the upper reaches of the study area. It is well known that these constituents result from shallow water effects, which cause energy transfer from principal tidal constituents to new frequencies that are multiples of the original frequencies [32, 33]. Figure (4) shows that the contribution of semidiurnal frequency bands or constituents (MNS2, 2N2, N2, M2, L2, T2, S2, R2, K2, 2SM2) increases, while the contribution of diurnal constituents (O1, M1, P1, S1, and K1) clearly decreases inland. Table 1 presents the phase shift variation of tidal constituents: the results indicate that only minor phase shifts were observed for the principal diurnal constituents, whereas the principal semidiurnal constituents exhibited comparatively larger phase variations. In contrast, substantial variability was observed for the shallow-water constituents as a result of nonlinear interactions. The phase difference of a tidal constituent reflects its propagation speed within a tidal system [34].

The phase difference of K1 is 30.34° (Time of K1 (tK1= 23.93 hours)), indicating that this constituent requires approximately 121 minutes to propagate from the Khor Abdullah inlet to the Shatt Al-Basrah Regulator. The phase difference of O1 is 8.5° (tO1 = 25.81 hours), corresponding to a propagation time of approximately 36.5 minutes between the two stations. Similarly, the phase difference of P1 is 39.82° (tP1 = 24.06 hours), indicating that about 160 minutes are required for this constituent to travel from Station 1 to Station 2. For the M2 constituent, a phase difference of 52.19° (approximately 108 minutes) was observed, indicating that high tide at the Shatt Al-Basrah Regulator occurs about 108 minutes after it occurs at the Khor Abdullah entrance. Correspondingly, the phase difference of S2 is 75.53°, suggesting that approximately 151 minutes are required for this constituent to propagate from Station 1 to Station 2. Likewise, the phase difference of N2 is 34.55° (tN2 = 12.69 hours), indicating a propagation time of approximately 73 minutes between the two stations. Differences in the phase of tidal constituents between the study stations may be attributed to bathymetric variations along the study area and nonlinear interactions with the channel bed. Significant fluctuations were also observed in shallow-water constituents due to tidal wave distortion along the study area, resulting from interactions with uneven shallow bathymetry, nonlinear advection, and bottom friction.

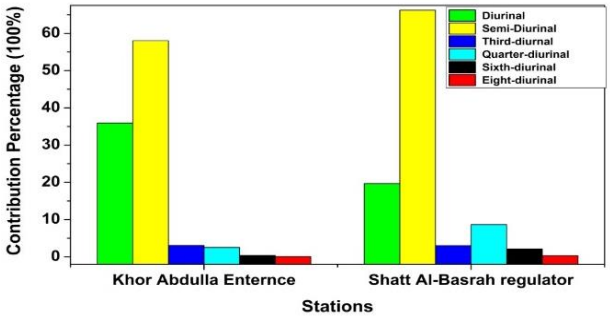

Figure (4): The percentage contribution of different frequency bands at the study stations.

The form factor ((Amp K1+Amp O1)/(Amp M2+Amp S2)) was 0.65 and 0.34 in station 1 and station 2, respectively. This decrease in form factor is due to the increase in the amplitude of semidiurnal constituents. However, in general, the form number falls within the range (0.25 < FN < 1.5), indicating that the study area is characterized by a mixed tide with a predominant semidiurnal constituent. This means that tidal wave energy is distributed across mixed frequencies between the diurnal and semidiurnal tide.

Conclusions

In this study, water level measurements at two locations northwest of the Arabian Gulf, Khor Abdulla entrance and Shatt Al-Basrah regulator, were utilized to highlight the characteristics of tidal waves that propagate from shallow coastal environments towards an inland direction. The analysis demonstrates that the tidal wave amplitude gradually increases as it propagates inland due to the convergent nature of the studied area. The study signifies that the constituent M2 has the highest amplitude at the two study stations. Correspondingly, the results illustrate that most constituents undergo an amplification as the tidal wave propagates towards the inland direction. The semi-diurnal tidal constituents M2, S2, and N2 were found to amplify towards the upstream with amplification rate was for S2 and M2, with 102% and 100%, respectively. The shallow water tidal constituents amplified from the station 1 to the upstream regions. The phase difference for M2 was recorded as 52.19° (approximately 108 minutes). This means that the high tide at the Shatt Al-Basrah regulator occurs 108 minutes after it occurs at the Khor Abdullah entrance. This finding is particularly relevant for navigation safety in waterways that support major commercial and oil ports.

Limitations and Future Work

This study provides important insights into tidal wave amplification and phase shift between Khor Abdullah and the Shatt Al-Basrah Regulator; however, some limitations remain.

1. Spatial coverage: Only two stations were analyzed. Adding intermediate sites would better capture spatial variability along the channel.
2. Temporal scope: The dataset covers one year (2022). Longer records are needed to evaluate interannual and decadal variability.
3. Meteorological forcing: Wind, atmospheric pressure, and river discharge were not considered. Incorporating these drivers could improve understanding of non-tidal contributions.
4. Numerical modeling: The study relied on observations and harmonic analysis. Coupling with hydrodynamic models would enable scenario testing under sea-level rise or engineering modifications.
5. Nonlinear tidal interactions: Overtides and compound tides were not examined in detail. Future work should assess their role in tidal asymmetry, sediment transport, and salt intrusion.
6. Anthropogenic influences: Dredging, regulator operation, and port construction were not evaluated. Quantifying these impacts would help separate natural and human-driven changes.
7. Regional context: Only local tide-gauge data were used. Integration with satellite altimetry and regional networks would provide broader spatial coverage.
8. Ecological linkages: Impacts on salinity intrusion, sediment dynamics, and ecosystem were beyond this study's scope. Interdisciplinary approaches could address these connections.

Disclosure Statement

- **Ethics clearance and participation consent:** NotApplicable.
- **Consent for publication:** Not Applicable.
- **Author's contribution:** Ali A. Lafta, Faez Y. Aleedani, and Abather J. Alhallaf: Study design and conception & Draft manuscript preparation. Ali A. Lafta: Computations, Data analysis, and result interpretation.
- **Conflicts of interest:** The authors declare that there is no conflict of interest regarding the publication of this article.
- **Funding:** No granted funding
- **Acknowledgements:** We would like to express our sincere gratitude to the scientific team who assisted us in conducting the field measurements as well as the General company of Port of Iraq for providing the data.

Open Access

References

1] Pastore DM, Peterson RN, Fribance DB, Viso R, Hackett EE. Hydrodynamic drivers of dissolved oxygen variability within a tidal creek in Myrtle Beach, South Carolina. Water. 2019; *11*(8), 1723; https://doi.org/10.3390/w11081723.

2] AlOsairi Y, Pokavanich T, Alsulaiman N. Three-dimensional hydrodynamic modeling study of reverse estuarine circulation: Kuwait Bay. Mar Pollut Bull. 2018; 127: 82–96; doi: 10.1016/j.marpolbul.2017.11.049.

3] Guo LC, van der Wegen M, Jay DA, Matte P, Wang ZB, Roelvink JA, He, Q. River-tide dynamics: Exploration of nonstationary and nonlinear tidal behavior in the Yangtze River estuary. J Geophys Res Oceans. 2015; 120:3499–3521; doi.org/10.1002/2014JC010491.

4] Lafta AA, Abdullah SS. Temporal Variability of Sea Surface Temperature in Iraq Marine Water, Northwest of Arabian Gulf. ILMU: KELAUTAN: Indones J Mar Sci. 2025; 30 (1): 145-151; doi.org/10.14710/ik.ijm.30.1.145-151.

5] Alhallaf AJB, Vilcáez J, Liang Y. Investigating the impact of meteorological factors on sea-level variability in the northwestern Arabian Gulf: A case study using deep learning and advanced statistical models. Ocean Mod. 2025; 102648; doi.org/10.1016/j.ocemod.2025.102648.

6] Puah JY, Haigh ID, Lallemant D, Morgan K, Peng D, Watanabe M, Switzer AD. Importance of Tides and Winds in Influencing the Nonstationary Behaviour of Coastal Currents in Offshore Singapore, Ocean Sci. 2024; 20(5): 1229–1246; doi.org/10.5194/os-20-1229-2024.

7] King E, Conley D, Masselink G, Leonardi N, McCarroll R, Scott T. The Impact of Waves and Tides on Residual Sand Transport on a Sediment-poor, Energetic, and Macrotidal Continental Shelf, J Geophys Res Oceans. 2019; 124(7): 4974–5002; doi.org/10.1029/2018JC014861.

8] Aubrey D, Speer P. A Study of Non-Linear Tidal Propagation in Shallow Inlet/Estuarine System Part I: Observations, Estuar Coast Shelf Sci. 1985; 21(2): 185–205; doi.org/10.1016/0272-7714(85)90096-4.

9] Boon JD. Secrets of the Tide: Tide and Tidal Current Analysis and Predictions, Storm Surges and Sea Level Trends. Horwood Publishing, Chichester. 2004.

10] Parker BB. Tidal analysis and prediction. Silver Spring, MD, NOAA NOS Center for Operational Oceanographic Products and Services, 378pp (NOAA Special Publication NOS CO-OPS 3). 2007.

11] Friedrichs CT, Aubrey DG. Non-Linear Tidal Distortion in Shallow Well-Mixed Estuaries: A Synthesis, Estuar Coast Shelf Sci. 1988; 27(5):521–545. doi.org/10.1016/0272-7714(88)90082-0.

12] Godin G. The Propagation of Tides up Rivers With Special Considerations on the Upper Saint Lawrence River. Estuar Coast Shelf Sci. 1999; 48(3): 307–324. doi.org/10.1006/ecss.1998.0422.

13] Munk WH, Cartwright DE. Tidal Spectroscopy and Prediction, Philosophical Transactions of the Royal Society of London. Series A, Math Phys Sci. 1966; 259(1105). doi.org/10.1098/rsta.1966.0024.

14] Cai H, Toffolon M, Savenije HHG, Yang Q, Garel E. Frictional interactions between tidal constituents in tide-dominated estuaries. Ocean Sci. 2018; 14:769–782. doi.org/10.5194/os-14-769-2018.

15] Munim MA, Mondal MS, Sakib MS, Hussain MA. Investigating spatiotemporal variation in tidal constituents along Bangladesh coast with harmonic analysis of high-resolution tidal data. Coast Eng J. 2025;67(3):417–432. doi.org/10.1080/21664250.2025.2513089.

16] Diouf A, Sakho I, Sow BA, Deloffre J, Seujip MS, Diouf MB, Lafite R. The Influence of Tidal Distortion on Extreme Water Levels in Casamance Estuary, Senegal. Estuar and Coast. 2025; 48, 42. doi.org/10.1007/s12237-024-01459-z.

17] Lafta AA. Investigation of Tidal Asymmetry in the Shatt Al-Arab River Estuary, Northwest of Arabian Gulf. Oceanologia. 2022; 64(2):376–386. https://doi.org/10.1016/j.oceano.2022.01.005.

18] Lafta AA, Altaei SA, Al-Hashimi NH. Impacts of Potential Sea-Level Rise on Tidal Dynamics in Khor Abdullah and Khor Al-Zubair, Northwest of Arabian Gulf. Earth Syst Environ. 2020; 4(1): 93–105. doi.org/10.1007/s41748-020-00147-9.

19] Alhumaidan ZA, Al-Jaberi MH, Al-Mosawi WM. Assessment the Subbottom Sedimentary Situation for Khor Abdullah, NW Arabian Gulf Using Sedimentary Coring Analysis and Sub-Bottom Profile Technique. Iraqi Geo J. 2023; 56 (2D):150-166. doi.org: 10.46717/igj.56.2D.12ms-2023-10-18.

20] Al-Mahdi AA, Mahmood AB. Some Features of Tidal Currents in Khor Abdullah, North West Arabian Gulf. J KAU: Mar Sci. 2010; 21(1). doi.org:10.4197/Mar.21-1.10.

21] Al-Hasem AM. Tidal Current Behaviors and Remarkable Bathymetric Change in the South-Western Part of Khor Abdullah, Kuwait, International Journal of Earth. Energy Environ Sci. 2018; 12(2):118–125. doi:10.5281/ZENODO.1315914.

22] Lafta AA. General Characteristics of Tidal Currents in the Entrance of Khor Abdullah, Northwest of Arabian Gulf. Oceanologia. 2023; 65(3):494–502. doi.org/10.1016/j.oceano.2023.03.002.

23] Alrawi S A, Jalal AD, Abdulhameed UH. Impact of Euphrates Water Levels on the Hydraulic Properties and Water Quality Parameter in Anbar Province, Iraq. An-Najah University Journal for Research - A (Natural Sciences). 2025; 39(2), 181–188. https://doi.org/10.35552/anujr.a.39.2.2399.

24] Lafta AA. Influence of Atmospheric Forces on Sea-Surface Fluctuations in Iraq Marine Water, Northwest of Arabian Gulf. Arab J Geosci. 2021; 14(16):1639. doi.org/10.1007/s12517-021-07874-x.

25] Adcock AA, Draper S. Power extraction from tidal channels – Multiple tidal constituents, compound tides and overtides. Renew Energy. 2014; 63:797-806. doi.org/10.1016/j.renene.2013.10.037.

26] Gerkema T. Tidal constituents and the harmonic method. An introduction to tides. Cambridge University Press. 2019; 60–86. doi.org/10.1017/9781316998793.005

27] Pous S, Carton X, Lazure P. A Process Study of the Tidal Circulation in the Persian Gulf. Open J Mar Sci. 2012; 02 (04): 131–40. doi.org/10.4236/ojms.2012.24016.

28] Yoon BII, Woo S-B. (2018) On the response of Shallow-water tidal regime by geological characteristic of waterway and Man-made structures in a macrotidal estuary: Han river estuary (Korea). J Coast Res. 2018; 85: 16-20. https://doi.org/10.2112/SI85-004.1.

29] Yuliardi AY, Heltria S, Taj K, Natih N. M. The amplitudes and phases of tidal constituents from harmonic analysis at two stations in the Gaspar Strait of Bangka Belitung. J Fish Mar Res. 2022; 18(1):10-19. doi.org/10.20884/1.oa.2022.18.1.893

30] Mandal S, Sil S, Gangopadhyay A, Jena BK, Venkatesan R. On the nature of tidal asymmetry in the Gulf of Khambhat, Arabian sea using HF radar surface currents, Estuarine. Coast Shelf Sci . 2020; 232. doi.org/10.1016/j.ecss.2019.106481.

31] Mahavadi TF, Seiffert R, Kelln J, Frohle P. Effects of sea level rise and tidal flat growth on tidal dynamics and geometry of the Elbe estuary. Ocean Sci. 2024; 20:369–388. doi: 10.5194/os-20-369-2024.

32] Hoitink A, Hoekstra, P, Van Maren D. Flow Asymmetry Associated with Astronomical Tides: Implications for the Residual Transport of Sediment. . J Geophys Res Oceans. 2003; 108(C10). doi.org/10.1029/2002JC001539.

33] Gallo MN, Vinzon SB. Generation of overtides and compound tides in Amazon estuary. Ocean Dyn. 2005; 55, 441–448. doi.org/10.1007/s10236-005-0003-8.

34] Hicks SD. Understanding Tides. NOAA, National Ocean Service. 2006.